Journal of Photochemistry and Photobiology A: Chemistry 224 (2011) 80–90

Contents lists available at SciVerse ScienceDirect

Journal of Photochemistry and Photobiology A: Chemistry

journal homepage: www.elsevier.com/locate/jphotochem

Theoretical analyses of photoinduced electron transfer in medium chain acyl-CoA dehydrogenase: Electron transfer in the normal region

Kiattisak Lugsanangarm[a], Somsak Pianwanit[a,b], Sirirat Kokpol[a,b,*], Nadtanet Nunthaboot[c], Haik Chosrowjan[d], Seiji Taniguchi[d], Fumio Tanaka[a,d,**]

[a] Department of Chemistry, Faculty of Science, Chulalongkorn University, Bangkok 10330, Thailand
[b] Center of Excellence for Petroleum, Petrochemicals, and Advanced Materials, Chulalongkorn University, Bangkok 10330, Thailand
[c] Department of Chemistry, Faculty of Science, Mahasarakham University, Mahasarakham 44150, Thailand
[d] Division of Laser BioScience, Institute for Laser Technology, Utsubo-Honmachi, 1-8-4, Nishiku, Osaka 550-0004, Japan

ARTICLE INFO

Article history:
Received 23 June 2011
Received in revised form 22 August 2011
Accepted 9 September 2011
Available online 18 September 2011

Keywords:
Medium chain acyl-CoA dehydrogenase
Photoinduced electron transfer
Kakitani and Mataga theory
Molecular dynamic simulation
Normal region

ABSTRACT

Medium chain acyl-CoA dehydrogenase (MCAD) binds flavin adenine dinucleotide (FAD) as cofactor, and catalyze α,β-dehydrogenation of fatty acid acyl-CoA conjugates as the first step of β-oxidation of fatty acids in mitochondria. The dynamic properties of geometrical factors as distances between isoalloxazine (Iso) and the aromatic amino acids of Trp and Tyr were studied by molecular dynamic (MD) simulation. The center-to-center distances (R_c) between Iso and aromatic amino acids were shortest in Tyr365 (0.99 nm) and then in Trp156 (1.00 nm), Tyr123 (1.29 nm), Tyr362 (1.42 nm). The Iso moiety was buried inside the protein, and surrounded by rigid and hydrophobic amino acids. The motions of the aromatic amino acids were suggested to be cooperative and synchronized with each other at some places in the protein. H-bonds were formed between Iso and Tyr123, Val125, Thr126 and Thr158. Photoinduced electron transfer (ET) from aromatic amino acids to the excited Iso (Iso*) was analysed from the reported ultrafast fluorescence dynamics of MCAD with Kakitani and Mataga (KM) theory. The ET rate was fastest from Trp156, and then from Tyr365, Trp47, Tyr302 and Trp165 in this order. Physical constants contained in KM theory were determined by a best-fit procedure between the observed and calculated fluorescence decays. Most of those quantities were similar to those derived from other flavoproteins. The free energy related to electron affinity of Iso* (G^0_{Iso}) and dielectric constant (ε_0) were, however, quite low compared to their mean values among four other flavoproteins, which was elucidated by the low polarity around Iso. The energy gap law of ET was examined and revealed that ET in MCAD takes place in the normal region.

1. Introduction

Acyl-CoA dehydrogenases constitute a family of flavoproteins that catalyze the α,β-dehydrogenation of fatty acid acyl-CoA conjugates with various carbon-chain lengths, and are essential for β-oxidation of fatty acid in mitochondria in cells [1,2]. The importance of such acyl-CoA dehydrogenases is illustrated, for example, by that genetic deficiencies in acyl-CoA dehydrogenase function are lethal, causing sudden infant death syndrome (SIDS) [3]. Acyl-CoA dehydrogenases contain flavin adenine dinucleotide (FAD) as a cofactor. The FAD in the proteins is reduced by two hydrogen atoms from the acyl-CoA, and then transports the electrons to the electron transferring flavoprotein. Since the three-dimensional structure has already been determined by X-ray diffraction method [4], medium chain acyl-CoA dehydrogenase (MCAD; 396 amino acids with Mw 47 kDa) is the best-studied member of the class and serves as a model for the study of their catalytic mechanisms. The isoalloxazine ring (Iso) of FAD in MCAD forms a charge transfer complex (CT) with various substrates during the enzymatic reaction [1,2]. The reaction mechanism has been studied through CT by various physico-chemical techniques, including Resonance Raman spectroscopy [5], ^{13}C-NMR spectroscopy and molecular orbital calculation (MO) [6].

Ultrafast fluorescence dynamics of several flavoproteins, including MCAD, have been studied by a fluorescence up-conversion method [7–10]. These flavoproteins appear practically non-fluorescent, but the fluorescence was found to decay in the sub-picosecond time domain upon excitation with very short pulsed laser (0.1 ps of pulse width). Such fast decays were ascribed

* Corresponding author at: Department of Chemistry, Faculty of Science, Chulalongkorn University, Bangkok 10330, Thailand.
** Corresponding author at: Department of Chemistry, Faculty of Science, Chulalongkorn University, Bangkok 10330, Thailand. Tel.: +66 858527182.
E-mail addresses: siriratkokpol@gmail.com (S. Kokpol), tfumio@yahoo.com (F. Tanaka).

1010-6030/$ – see front matter © 2011 Elsevier B.V. All rights reserved.
doi:10.1016/j.jphotochem.2011.09.010

to photoinduced electron transfer (abbreviation ET in the present work is used for electron transfer in the excited state) from Trp and/or Tyr to the excited Iso (Iso*) [11,12].

Since Marcus first proposed an electron transfer theory [13–15], it has been improved by many workers [16–20]. These theories are, however, modeled for electron transfer processes in bulk solution. Electron transfer phenomena in proteins have been precisely described [21,22]. However, it has been difficult to study the ET mechanism by determining every physical constant in the theories, because the theories contain several unknown parameters. We have been trying to establish a method for analysis of ET in flavoproteins, with the atomic coordinates being obtained by molecular dynamic (MD) simulation, and Kakitani and Mataga theory (KM theory) [20]. Every physical constant in the KM theory were determined by analyzing fluorescence dynamics of flavoproteins, according to a non-linear least-square method [23–27]. The non-linear least-square method has been useful to determine several parameters contained in a theory, which cannot be determined by experiments, and has been used for Global analysis type methods [28]. Once the method is established, it may also be applied for electron transfer processes in the dark.

Ultrafast fluorescence dynamics of MCAD were reported to have a 1.9 ps average lifetime [7]. However, the whole picture of ET in MCAD has not yet been made clear. In the present work, the ET mechanism from Trp or Tyr to Iso* in MCAD was analysed to determine the physical constants contained in the ET theory from the ultrafast fluorescence dynamics of MCAD with the atomic coordinates obtained by MD, and compared with ET mechanisms of other flavoproteins. We hope that this contribution will be useful especially for engineering flavoprotein redox potentials, current and prospective biotechnological and bioelectronics applications, including biosensors.

2. Methods of analyses

2.1. Molecular dynamics simulation

MD simulations were started from a MCAD-FAD complex which has been determined by the X-ray crystallographic methods (pdb code: 3MDD) [4]. All heavy missing atoms in the initial structure were added using Discovery Studio 2.0 software (Website, http://www.discoverystudios.com). All hydrogen atoms of the protein were added using the LEaP module of the Amber 10 software package [29]. The force field parameters of FAD were given by Antechamber and the Gaff [29]. Charges of atoms in FAD were obtained by Gaussian 03 [30] with the Hartree–Fock method and 6–31G* basis set. The MCAD was minimized with 1000 steps of the steepest decent minimization, followed by 2000 steps of conjugate gradient minimization to remove the geometrical strain. The protein then was solvated by 14926 TIP3P water molecules. To neutralize the negative charges of the system, 3 sodium counter ions were added to the regions with the largest positive Coulombic potentials. Subsequently, secondary minimization of the whole system was carried out with 2000 steps of steepest decent and 3000 steps of conjugate gradient methods. This minimized and solvated system was then used as the starting structure for all the subsequent MD calculations. Afterwards, the whole system was heated from 100 K to 298 K over 25 ps and was further equilibrated under periodic boundary conditions. The MD systems were set under the normal temperature and pressure (NPT) with a constant pressure of 1 atm and constant temperature of 298 K. The SHAKE algorithm [31] was employed to constrain all bonds involving hydrogen atoms. The long-range electrostatic interactions in periodic boundary conditions were described with a particle mesh Ewald method [32] with a spherical cutoff of 10.0 Å for non-bonded interactions. The MD calculation was carried out for 7 ns of the simulation time with 0.002 ps time step. The stability of the system was observed by global root of mean square deviation (RMSD) and MD snapshots were collected from 5 ns to 7 ns (net 2 ns) of the production phase with 10 fs intervals, giving 200,000 snapshots for the analysis of ET in MCAD (see Fig. S1 in Supplemental Material for time-evolution of RMSD).

The residue-based root mean square fluctuation (RMSF) of each amino acid, which indicates the structural flexibility for each amino acid residue, was obtained by superposition of the trajectory conformations and the reference conformation of amino acid over equilibrium MD snapshots using the ptraj module of the Amber program. The RMSF defined as $\mathrm{RMSF}(i) = \sqrt{\left\langle (R_i - \langle R_i \rangle)^2 \right\rangle}$, where R_i is the position vector of atom i (in this study, the Cα, N, and O atoms coordinates were evaluated). The chevron brackets represent the time average over the whole trajectory.

2.2. ET theory

The original Marcus ET theory [13–15] has been modified in various ways [16–20]. In the present analysis, the Kakitani and Mataga (KM) theory [20] was used, because it is applicable for both adiabatic and non-adiabatic ET process. In fact, the structure of protein is always dynamic. Therefore, the adiabatic and non-adiabatic properties can partially incorporate all the time. The ET analyses by using KM theory have been found to give satisfactory results for static analyses in several flavoproteins [10,33,34], and dynamic ET analyses in FMN binding protein (FMN-bp) [23,24,27] and the anti-repressor of the photosynthetic gene expression regulon (AppA). The ET rate described by KM theory is expressed by Eq. (1).

$$k_{\mathrm{ET}}^{j} = \frac{\nu_0^q}{1 + \exp\left\{\beta^q (R_j - R_0^q)\right\}} \times \sqrt{\frac{k_{\mathrm{B}}T}{4\pi\lambda_{\mathrm{S}}^{qj}}} \exp\left[-\frac{\left\{ \Delta G_q^0 - e^2/\varepsilon_0^q R_j + \lambda_{\mathrm{S}}^{qj} + \mathrm{ES}_j \right\}^2}{4\lambda_{\mathrm{S}}^{qj} k_{\mathrm{B}} T} \right] \quad (1)$$

Here k_{ET}^{j} is the ET rate from a donor j to Iso*, and index q denotes Trp or Tyr. ν_0^q is an adiabatic frequency, β^q is the ET process coefficient. R_j and R_0^q is the donor j–Iso distance and its critical distance for the ET process, respectively. R_j is expressed as a center-to-center (R_{c}) distance rather than edge-to-edge (R_{e}) distance [10,23–27,33,34]. The ET process is adiabatic when $R_j < R_0^q$, and non-adiabatic when $R_j > R_0^q$. k_{B}, T and e are Boltzmann constant, temperature and electron charge, respectively. ES_j is electrostatic (ES) energy, which is described below. MCAD contains 4 Trp and 17 Tyr residues. In the present work the ET rates from all of these aromatic amino acids to Iso* were taken into account for the analysis.

$\lambda_{\mathrm{S}}^{qj}$ is the solvent reorganization energy [10,11] of the ET donor q and j, and is expressed as Eq. (2).

$$\lambda_{\mathrm{S}}^{qj} = e^2 \left(\frac{1}{2a_{\mathrm{Iso}}} + \frac{1}{2a_q} - \frac{1}{R_j} \right) \left(\frac{1}{\varepsilon_\infty} - \frac{1}{\varepsilon_0^q} \right) \quad (2)$$

where a_{Iso} and a_q are the radii of Iso and Trp or Tyr, with these reactants being assumed to be spherical, and ε_∞ and ε_0^q are optical and static dielectric constants. The static dielectric constants for electrostatic (ES) energy between Trp156 ($\varepsilon_0^{\mathrm{W}}$) or Tyr365 ($\varepsilon_0^{\mathrm{Y}}$) cation and Iso anion, $-e^2/\varepsilon_0^q R_j$, and the solvent reorganization energies for these ET donors were separately evaluated, because the values of R_{c} for these donors are quite close within 1 nm, and hence amino acids rarely exist between the donors and acceptor. This

situation may be quite different from the ES energy between the ionic species of photoproducts and the other ionic groups in the protein as described below. The distances between Iso anion or the donor cations and the ionic groups were longer than those between the donor cations and Iso anion, so that many amino acids were existed between the ionic photoproducts and the other ionic groups in the protein. The optical dielectric constant used was 2.0. The radii of Iso (a_{Iso}), Trp (a_{Trp}) and Tyr (a_{Tyr}) were determined as before [20,21], to be 0.224 nm, 0.196 nm and 0.173 nm, respectively.

The standard free energy change was expressed with the ionization potential of the ET donor, E^q_{IP}, as Eq. (3).

$$\Delta G^0_q = E^q_{IP} - G^0_{Iso} \tag{3}$$

Here, G^0_{Iso} is standard Gibbs energy related to electron affinity of Iso*. The values of E^q_{IP} for Trp and Tyr were 7.2 eV and 8.0 eV, respectively [35].

2.3. Electrostatic energy in the MCAD

Protein systems contain many ionic groups, which may influence the ET rate. MCAD contains Iso as the ET acceptor, with four Trp residues (Trp47, Trp156, Trp165 and Trp307) and 17 Tyr residues (Tyr32, Tyr38, Tyr79, Tyr104, Tyr110, Tyr123, Tyr148, Tyr166, Tyr267, Tyr302, Tyr317, Tyr318, Tyr325, Tyr350, Tyr362, Tyr365 and Tyr384) as potential ET donors. The FAD cofactor in MCAD has 2 negative charges at the pyrophosphate, whilst MCAD itself contains 31 Glu, 16 Asp, 25 Lys and 21 Arg residues.

The ES energy between Iso anion or donor cation j and all other ionic groups in the protein is expressed by Eq. (4)

$$E(j) = \sum_{i=1}^{31} \frac{C_j \cdot C_{Glu}}{\varepsilon_0 R_j(\mathrm{Glu}-i)} + \sum_{i=1}^{16} \frac{C_j \cdot C_{Asp}}{\varepsilon_0 R_j(\mathrm{Asp}-i)} + \sum_{i=1}^{25} \frac{C_j \cdot C_{Lys}}{\varepsilon_0 R_j(\mathrm{Lys}-i)} + \sum_{i=1}^{21} \frac{C_j \cdot C_{Arg}}{\varepsilon_0 R_j(\mathrm{Arg}-i)} + \sum_{i=1}^{2} \frac{C_j \cdot C_P}{\varepsilon_0 R_j(P-i)} \tag{4}$$

where $j=0$ for the Iso anion, 1–4 for the Trp cations and 5–21 for the Tyr cations. C_j is the charge of the aromatic ionic species j, that is $-e$ for $j=0$ and $+e$ for $j=1$–21. C_{Glu} ($=-e$), C_{Asp} ($=-e$), C_{Lys} ($=+e$), C_{Arg} ($=+e$) and C_P ($=-e$) are the charges of the Glu, Asp, Lys and Arg residues plus the phosphate anions, respectively. We assumed that these groups are all in an ionic state in solution. The distances between the aromatic ionic species j and the ith Glu ($i=1$–31) are denoted as R_j (Glu $-$ i), whilst the distances between the aromatic ionic species j and the ith Asp ($i=1$–16) are denoted as R_j (Asp $-$ i), and so on. The dielectric constant in this *ES* energy was ε_0 which was separately evaluated from ε^W_0 or ε^Y_0. The reason was described above.

ES_j in Eq. (1) was expressed as follows:

$$ES_j = E(0) + E(j) \tag{5}$$

Here j is from 1 to 21, and represents jth ET donor as described above.

2.4. Fluorescence decays

The observed fluorescence decay function of MCAD was reported by Mataga et al. [7], and is expressed by Eq. (6) in Method A.

$$F^f_{obs}(t) = 0.837\exp\left(\frac{-t}{0.299}\right) + 0.127\exp\left(\frac{-t}{1.09}\right) + 0.036\exp\left(\frac{-t}{42}\right) \tag{6}$$

The lifetimes were indicated in unit of ps. The calculated decay function is expressed by Eq. (7).

$$F^f_{calc}(t) = \left\langle \exp - \left\{ \sum_{j=1}^{21} k^j_{ET}(t') \right\} t \right\rangle_{AV} \tag{7}$$

Fluorescence decays were calculated up to 10 ps. The $\langle\ldots\rangle_{AV}$ means the averaging procedure of the exponential function in Eq. (7) over t' up to 2 ns with 0.1 ps time intervals. In Eq. (7) we assumed that the decay function at every instant of time, t', during the MD time range can be always expressed by the exponential function. The present method is mathematically equivalent to the reported one [36] when the time range (2 ns) of MD data is much longer than one (10 ps) of fluorescence data. The mathematical basis of this approach is described in Supplemental Material.

In Method A the unknown ET parameters (ν^q_0, β^q, and R^q_0 for Trp and Tyr, G^0_{Iso} and ε_0) contained in the KM theory were determined so as to obtain the minimum value of χ^2_A, defined by Eq. (8), by means of a non-linear least squares method, according to the Marquardt algorithm, as previously reported [23–27].

$$\chi^2_A = \frac{1}{N}\sum_{i=1}^{N} \frac{\left\{F^f_{calc}(t_i) - F^f_{obs}(t_i)\right\}^2}{F^f_{calc}(t_i)} \tag{8}$$

Here N denotes number of time intervals of the fluorescence decay, and was 500 with the time intervals of 0.02 ps.

In Method B, the observed fluorescence decay curve instead of the observed decay function expressed by Eq. (6), as in Eq. (9).

$$F^c_{calc}(t) = \int_0^t P(t-t')F^f_{calc}(t')dt' \tag{9}$$

Eq. (9) shows a convolution of the calculated decay function $F^f_{calc}(t')$ given by Eq. (7) with an instrumental response, $P(t-t')$, which is illustrated in the reported work [7]. The unknown ET parameters were determined so as to obtain the minimum value of χ^2_B defined by Eq. (10).

$$\chi^2_B = \frac{1}{N}\sum_{i=1}^{N} \frac{\left\{F^c_{calc}(t_i) - F^c_{obs}(t_i)\right\}^2}{F^c_{calc}(t_i)} \tag{10}$$

$F^c_{obs}(t)$ indicates the observed decay curve reported [7]. The deviation between the observed and calculated fluorescence decays were obtained by Eq. (11).

$$\mathrm{Deviation}(t_i) = \frac{\left\{F_{calc}(t_i) - F_{obs}(t_i)\right\}}{\sqrt{F_{calc}(t_i)}} \tag{11}$$

In Eq. (11) $F_{obs}(t)$ denotes $F^f_{obs}(t)$ in Method A or $F^c_{obs}(t)$ in Method B, and $F_{calc}(t)$, $F^f_{calc}(t)$ in Method A or $F^c_{calc}(t)$ in Method B.

3. Results

3.1. Geometrical factors near FAD binding site

The protein structure of MCAD at the FAD binding site is shown in Fig. 1. The mean R_c and R_e distances and the inter-planar angles between Iso and aromatic amino acid residues and the adenine moiety over a MD time range of 0.1 ps time intervals are listed in Table 1. Tyr365 displayed the shortest R_c from Iso, and followed by Trp156, Tyr362, Tyr123, Tyr38 and Tyr166. These six amino acid residues were also the closest to Iso by R_e, although the ranked order was slightly different from that of R_c. The time-dependent changes in the R_c of the four Trp residues revealed that the R_c of

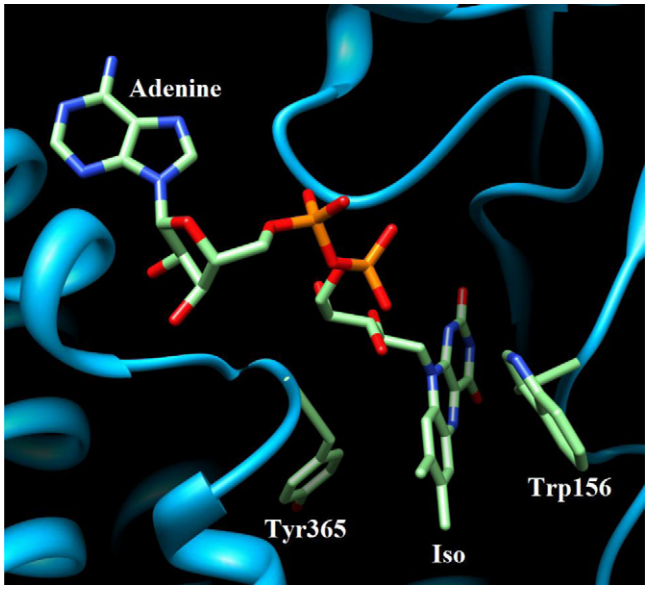

Fig. 1. The protein structure of MCAD at the FAD binding site.

Trp156 displayed a tendency to decrease a little with time, whilst the other three Trp residues increased a little with time (Fig. 2). Instantaneous fluctuations in R_c were, however, rather small. The corresponding time-dependent changes in the R_c of the five closest Tyr residues (based on R_c values, see Table 1) revealed that the R_c values increased a little with time (Fig. 3). The time-dependent changes in the inter-planar angles between Iso and the four Trp amino acid residues showed a decrease from around 75° to 40° for Trp47 at 0.4 ns, whilst Trp307 increased from −90° to −60° at around 0.2 ns. Although the angles of the other Trp residues were relatively constant (Fig. 4), all showed remarkable instantaneous fluctuations by as much as ±20°. The mean angles are listed in Table 1. The time-dependent changes in the angles of the five selected Tyr residues (see above) showed that Tyr123 tends to increase from −70° to −50° with time, whilst Tyr362 decreased from 50° to 30° (Fig. 5).

Table 1
Geometrical factors between Iso and adenine/aromatic amino acids.[a]

Adenine and amino acid	R_c (nm)	R_e (nm)	Inter-planar angle (°)
Adenine	1.64	1.15	85.0
Trp47	2.68	1.79	42.1
Trp156	1.00	0.30	−33.6
Trp165	2.08	1.15	−80.6
Trp307	3.20	2.62	−74.0
Tyr32	2.29	1.60	65.2
Tyr38	1.64	0.96	57.3
Tyr79	2.58	1.92	−110.8
Tyr104	3.41	2.51	−52.9
Tyr110	2.54	1.67	64.6
Tyr123	1.29	0.28	−61.8
Tyr148	2.97	1.99	−61.8
Tyr166	1.69	0.78	74.7
Tyr267	3.42	2.81	87.8
Tyr302	2.29	1.83	24.2
Tyr317	2.74	2.18	−50.7
Tyr318	2.82	2.23	−82.5
Tyr325	2.55	1.99	−34.5
Tyr350	3.19	2.45	−39.9
Tyr362	1.42	0.83	32.2
Tyr365	0.99	0.37	−21.8
Tyr384	3.50	2.93	−4.3

[a] The mean of the geometrical factors are derived from over 20,000 snapshots with 0.1 ps time intervals.

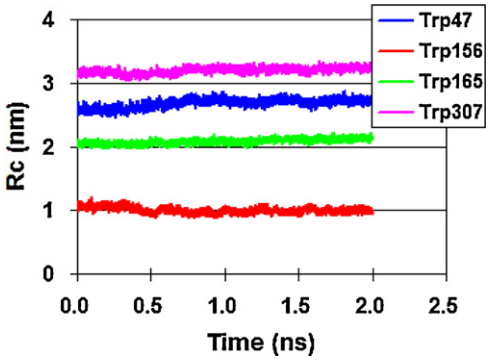

Fig. 2. Center-to-center distances (R_c) between Iso and the four Trp residues.

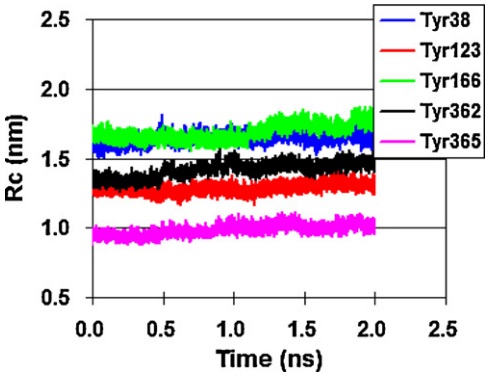

Fig. 3. Center-to-center distances (R_c) between Iso and the five selected Tyr residues (those closest to the Iso, as defined by R_c values).

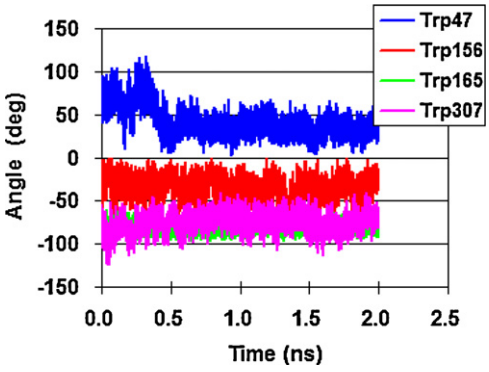

Fig. 4. Inter-planar angles between Iso and the four Trp residues.

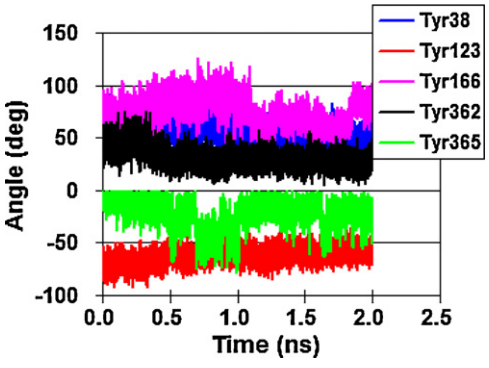

Fig. 5. Inter-planar angles between Iso and the five selected Tyr residues.

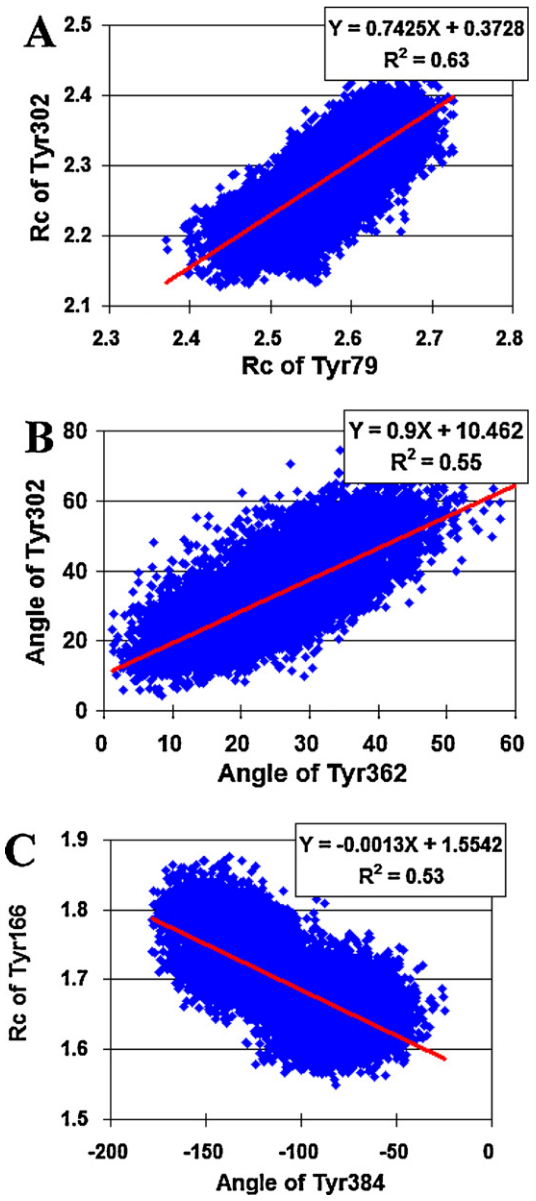

Fig. 6. Correlation between two independent geometrical factors. The R_c and inter-planar angle between Iso and the three indicated aromatic amino acid pairs. Pearson's correlation coefficients were 0.825 in A, 0.740 in B and −0.785 in C. Red solid lines indicate the linear regression, with the equation and R^2 coefficient shown in the insert. (For interpretation of the references to color in this figure legend, the reader is referred to the web version of the article.)

3.2. Correlation between geometrical factors relative to Iso

Correlations between the R_c and inter-planar angle between Iso and the aromatic amino acids were examined with analysis using Pearson correlation coefficients and linear regression. Fig. 6 shows the correlations of the three paired factors that had Pearson correlation coefficients higher than 0.7 (absolute value). This shows that (i) the relationship between the R_c values of Tyr302 and Tyr79, with a reasonably high Pearson correlation coefficient (0.825) and linear regression (Fig. 6A); (ii) the inter-planar angles of Tyr302 and Tyr362, again with a reasonable Pearson's correlation coefficient (0.740) (Fig. 6B); (iii) the R_c of Tyr166 and the inter-planar angle of Tyr384, which were inversely related with a Pearson correlation coefficient of −0.785 (Fig. 6C). The other pairs with a relatively high Pearson correlation coefficient, defined as >0.7 for R_c and >0.6 in absolute values for the inter-planar angle, are listed in Table 2. Some

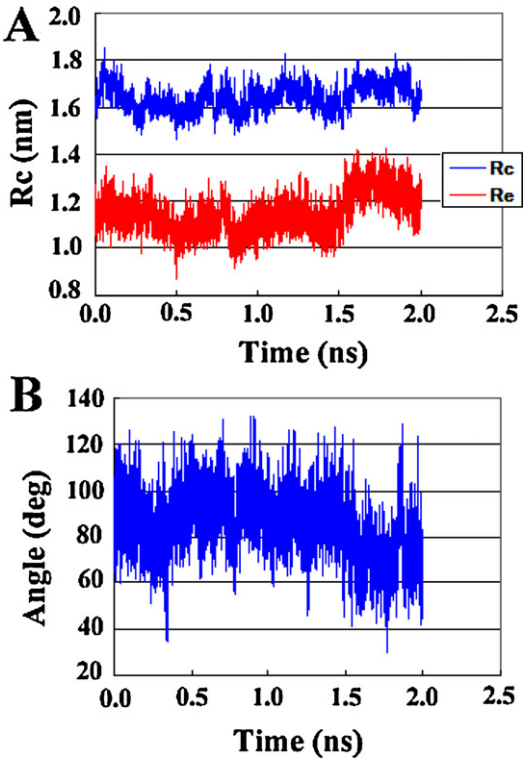

Fig. 7. Dynamics of the FAD geometry within the MCAD protein. (A) The R_c and R_e between Iso and the adenine moiety and (B) the inter-planar angle between Iso and adenine.

pairs of amino acids were found to be correlated, which are spatially located at distant places to each other and with no geometrically apparent relationship between them.

3.3. Dynamics of FAD structure

The time-dependent changes in the R_c and R_e values between Iso and the adenine moiety are shown in Fig. 7A, where the R_c values varied from 1.45 nm to 1.75 nm, which is much more marked compared to that observed for the Trp or Tyr amino acid residues. It seemed to display a long period fluctuation in sub-nanoseconds, in addition to the instantaneous fluctuation. The time-dependent changes in the inter-planar angle between Iso and adenine (Fig. 7B) displayed marked fluctuation compared to Trp buried in the protein.

3.4. Rigid and flexible parts of MCAD

Residue RMSF can be used to measure protein flexibility, and the results for MCAD are shown in Fig. 8 where the

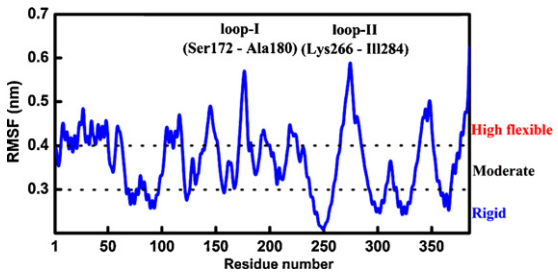

Fig. 8. Residue RMSF in MCAD. The RMSF (nm) of each amino acid residue of MCAD. The rigid and flexible parts were defined by having a residue RMSF of <0.3 nm and >0.4 nm, respectively.

Table 2
Pearson correlation coefficients between the two paired geometrical factors (R_c, R_e and inter-planar angle) of the aromatic amino acids relative to Iso for those pairings with a significant correlation (>0.7 for R_c and R_e and >0.6 for interplanar angles, respectively).[a]

Geometrical factor (A)	Geometrical factor (B)							
	Amino acid	Correlation coefficient	Amino acid	Correlation coefficient	Amino acid	Correlation coefficient	Amino acid	Correlation coefficient
^{R}Trp47	^{R}Tyr32	0.709	^{R}Tyr79	0.764	^{R}Tyr302	0.723	^{R}Tyr362	0.735
^{R}Trp165	^{A}Tyr384	−0.656						
^{R}Trp307	^{R}Tyr302	0.733	^{R}Tyr318	0.748				
^{R}Tyr32	^{R}Tyr38	0.718	^{R}Tyr79	0.745				
^{R}Tyr79	^{R}Tyr267	0.729	^{R}Tyr302	0.794	^{R}Tyr362	0.825	^{R}Tyr365	0.713
^{R}Tyr166	^{A}Tyr384	−0.727						
^{R}Tyr302	^{R}Tyr318	0.733	^{R}Tyr325	0.722	^{R}Tyr362	0.821	^{R}Tyr365	0.718
^{R}Tyr318	^{R}Tyr362	0.720						
^{R}Tyr325	^{R}Tyr362	0.749						
^{R}Tyr350	^{R}Tyr362	0.718	^{A}Tyr384	−0.637				
^{R}Tyr362	^{R}Tyr365	0.814	^{A}Tyr362	−0.652	^{A}Tyr384	−0.603		
^{R}Tyr384	^{A}Tyr384	−0.785						
^{A}Trp47	^{A}Tyr302	0.620	^{A}Tyr362	0.675				
^{A}Tyr38	^{A}Tyr123	−0.611	^{A}Tyr302	0.601	^{A}Tyr317	0.214		
^{A}Tyr123	^{A}Tyr362	−0.682						
^{A}Tyr302	^{A}Tyr318	0.620	^{A}Tyr362	0.740				

[a] Pearson correlation coefficients are listed between geometrical factors A and B. R and A denotes the R_c and interplanar angle between Iso and indicated amino acid, respectively. Coefficients are listed only for those that are greater than 0.7 for R_c and 0.6 for the angle.

criteria used to define rigid and flexible amino acids was a RMSF residue of <0.3 nm and >0.4 nm, respectively. The RMSF values were highest (most flexible) at the Ser172–Ala180 (loop-I) and Lys266–Ile284 (loop-II) regions, and lowest (most rigid) around residue No. 250. Fig. 9A shows the locations of the rigid (blue) and flexible (red) amino acids. Rigid amino acids were Leu51–Pro57, Gly64–Gly102, Ala292–Trp307, Thr316–Gln332 and Asp358–Gly367, whilst flexible amino acids were Thr7–Leu63, Asn103–Pro118, Lys140–Asn155, Ser172–Ala180, Asp192–Gly199, Phe217–Glu225, Lys266–Ile284 and Gln339–Pro351. The lower panel in Fig. 9B shows a close view of the Iso binding site, which suggests that Iso is buried in some of the most rigid amino acids. The amino acid residues near (within 6 Å) Iso are Thr86, Ala90, Leu93, Tyr123–Thr126, Pro128, Gly129–Asp133, Trp156–Thr158, Asn204, Gln207, Thr212, Ile361, Ile364–Thr368, Gln370 and Ile371, which only Pro128, Gly129–Asp133, Thr368, Gln370 and Ile371 have the moderate flexibility. Fig. 9C shows a close view of adenine part of FAD. Adenine part was exposed into water layer at the protein–water interface, not buried in the protein, which is in accord with marked fluctuation of inter-planar angle between Iso and adenine as stated above (see Fig. 7B).

3.5. Hydrogen bonding interaction of FAD with surrounding amino acids

The hydrogen bonding (H-bond) interaction, represented as a percentage occupation, was determined with the following criteria: (1) the distance between proton donor (D) and acceptor (A) atoms was equal to or less than 0.35 nm and (2) the D–H···A angle was equal to or greater than 120°. The likely H-bond pairs found are listed in Table 3, and the likely H-bond interactions between FAD and the surrounding amino acids are shown as dotted lines together with the distances (Fig. 10A), and as the percentage occupations of potential H-bonds pairs (Fig. 10B). From these data it is concluded that major H-bonds are formed between Iso and the MCAD Tyr123, Val125, Thr126 and Thr158 residues. In addition, the O4 and N3H of Iso formed strong hydrogen bonds with water molecules, having 90% and 75.3% occupancy. The alcohol oxygen atoms of the ribityl chain form H-bonds with the MCAD Glu366NH/C2*O, Gly367NH/C4*O and Ser132O/C4* pairs (see Chart 1 for atom notations of FAD), whilst the oxygen atoms of the FAD pyrophosphate formed H-bonds with the peptide NH of the MCAD Gly131, Gly129 and Ser132 residues. On the other hand, only one hydrogen bond was found between adenine and Thr368 with 64.8% occupancy, but then again the adenine moiety has a much higher motional freedom in the water layer as discussed above.

3.6. Fluorescence dynamics and physical constants related to ET

The observed fluorescence decay of MCAD was analysed with two methods (Method A and Method B) described in Section 2. Fig. 11 shows the observed and calculated decays obtained by Method B. The ET parameters in KM theory determined by Method A were $\nu_0^{Trp} = 1164\,ps^{-1}$, $\nu_0^{Tyr} = 1.78\,ps^{-1}$, $\beta^{Trp} = 7.04\,nm^{-1}$, $\beta^{Tyr} = 0.677\,nm^{-1}$, $R_0^{Trp} = 0.738\,nm$, $R_0^{Tyr} = 1.63\,nm$, $G_{Iso}^0 = 6.23\,eV$, and $\varepsilon_0 = 4.22$, $\varepsilon_0^W = 2.54$, and $\varepsilon_0^Y = 2.27$. The ET parameters obtained by Method B were $\nu_0^{Trp} = 1135\,ps^{-1}$, $\nu_0^{Tyr} = 4.78\,ps^{-1}$, $\beta^{Trp} = 4.20\,nm^{-1}$, $\beta^{Tyr} = 0.606\,nm^{-1}$, $R_0^{Trp} = 0.786\,nm$, $R_0^{Tyr} = 1.18\,nm$, $G_{Iso}^0 = 6.18\,eV$, and $\varepsilon_0 = 3.29$, $\varepsilon_0^W = 2.71$, and $\varepsilon_0^Y = 2.13$. The decay was calculated with these quantities obtained by Method B. The values of χ_A^2 defined by Eq. (8) was 3.11×10^{-3}, and χ_B^2 obtained by Eq. (10) 1.25×10^{-2}. The value of χ_B^2 was much greater than one of χ_A^2. This may be ascribed to experimental variation in $F_{obs}^c(t)$. Deviations between $F_{obs}(t)$ and $F_{calc}(t)$ should increase when the observed intensities are used for the analysis, instead of the smooth decay function. The extent of the agreement between $F_{obs}(t)$ and $F_{calc}(t)$ may not be different much in both analyses with Method A and Method B. The physical constants of ET in MCAD were listed in Table 4, together with those in other flavoproteins for comparison. The mean values of the four systems (4 of flavodoxins, 3 of AppAs and 2 kind of FMN-bp) other than MCAD were $\nu_0^{Trp} = 1900\,ps^{-1}$, $\nu_0^{Tyr} = 1400\,ps^{-1}$, $\beta^{Trp} = 29\,nm^{-1}$, $\beta^{Tyr} = 7.2\,nm^{-1}$, $R_0^{Trp} = 0.64\,nm$, $R_0^{Tyr} = 0.98\,nm$, $G_{Iso}^0 = 8.6\,eV$. The values of ν_0^{Trp}, β^{Tyr} and G_{Iso}^0 in MCAD were quite lower than the respective mean values. The value of ε_0 should be dependent on the protein system. The value of ε_0 in MCAD was quite lower than those of other systems, 4.22 by Method A and 3.29 by Method B. The MCAD is an enzyme and binds substrates of fatty acid derivatives. To bind such hydrophobic substrates the protein must be hydrophobic. In fact Iso moiety was completely buried in the protein, and surrounded by Thr86, Ala90, Leu93, Tyr123, Cys124, Val125, Thr126, Pro128, Gly129, Ala130, Gly131, Ser132, Asp133, Trp156, Ile157, Thr158, Asn204, Gln207, Thr212, Ile361, Ile364, Tyr365, Glu366, Gly367, Thr368, Gln370,

Table 3
Percentage occupation of H-bonds between FAD and MCAD amino acid residues.[a]

No.	FAD atom	Residue	Distance (nm)/angle (°)	Percentage occupation	Moiety in FAD
1	O2	Thr126(NH)	0.29/168.6	100.0	Iso
2	N3H	Tyr123(O)	0.30/160.2	100.0	
3	N1	Thr126(OG)	0.28/166.6	99.8	
4	O2	Val125(NH)	0.34/152.9	98.8	
5	O4	Water(H)	0.27/167.2	90.8	
6	O2	Thr126(OG)	0.30/139.8	89.8	
7	N3H	Water(H)	0.37/133.6	75.3	
8	O4	Thr158(NH)	0.33/160.2	69.8	
9	C2*O	Glu366(NH)	0.30/166.9	99.4	Ribityl
10	C4*O	Gly367(NH)	0.31/157.7	98.0	
11	C4*O	Ser132(O)	0.28/174.3	65.5	
12	O^{P1}	Gly131(NH)	0.32/148.6	90.0	Pyrophosphate
13	$^{A}O^{P1}$	Gly129(NH)	0.32/150.6	82.5	
14	O^{P2}	Gly131(NH)	0.28/151.4	64.7	
15	O^{P2}	Ser132(NH)	0.30/163.5	62.3	
16	^{A}C3*O	Thr368(OH)	0.29/166.4	64.8	Adenine

[a] Atom notations in FAD are indicated in Chart 1. NH and O in the residues denote peptide NH and O. OG in Thr126 is the O atom in the side chain.

Ile371 (stated above, see Fig. 9) within 0.6 nm of the distances to Iso. Among these amino acids only Asp133 is ionic, and most of them are hydrophobic. The reason why ε_0 is low, may be elucidated by these facts.

The dielectric constants between Trp156 and Iso (ε_0^W) and between Tyr365 and Iso (ε_0^Y) were 2.5 and 2.3 by Method A, and 2.7 and 2.1 by Method B, respectively. These values were also quite low. In the recent work on FMN-bp [27], the dielectric constant between the ET donors and acceptor was separately evaluated from those in the entire proteins, and displayed lower than those of the entire proteins.

3.7. ET rates and ES energy in MCAD

The time-dependent changes in the ET rates from five aromatic amino acids (one of the four Trp and four of the Tyr residues) are shown in Fig. 12, whilst the natural logarithm of the mean ET rates is listed in Table 5. The ET rate from Trp156 was the fastest among the 21 aromatic amino acids, although the values of R_c were almost identical between Trp156 (1.00 nm) and Tyr365 (0.99 nm), followed by Tyr123 (1.29 nm), Tyr362 (1.42 nm) and Tyr38 (1.64 nm) and Tyr166 (1.69 nm) in this order.

Fig. 13 shows time-evolution of net *ES* energies between the photoproducts and other ionic groups in the protein, given by Eq. (5). E_{iso} was always positive, which is ascribed to the repulsion energy between the Iso anion and the two negative charges at pyrophosphate. The ES energies of the ET donors were all negative. Mean net ES energies (ES_j) given by Eq. (5) over the MD time range (Table 5) were lowest in Tyr302 (−1.168 eV) and highest in Tyr317 (0.815 eV), whilst the ES energies ($-e^2/\varepsilon_0 R_j$) between the Iso anion and donor cations (Table 5) were lowest in Tyr365 (−0.695 eV) and highest in Tyr384 (−0.125 eV). ΔG_q^0 were 0.74 eV and 1.54 eV for all Trp and Tyr residues, respectively. The values of λ_S^{qj} (Table 5) were lowest in Tyr365 (0.14 eV), and highest in Tyr384 (0.1.37 eV).

3.8. Energy gap law

The total free energy gap is expressed by Eq. (12).

$$-\Delta G_T^0(j) = -ES_j + \frac{e^2}{\varepsilon_0 R_j} - \Delta G_q^0 \tag{12}$$

The original energy law is expressed by Eq. (13), when pre-exponential terms and λ_S^{qj} are not changed appreciably with ET donors.

$$\ln k_{ET}^j \propto -\left\{\lambda_S^{qj} + \Delta G_T^0(j)\right\}^2 \tag{13}$$

Table 4
Comparison of physical constants of ET between MCAD and other flavoproteins.[a]

System	Trp			Tyr								
	ν_0^{Trp} (ps^{-1})	β^{Trp} (nm^{-1})	R_0^{Trp} (nm)	ν_0^{Tyr} (ps^{-1})	ν_0^{Tyr} (nm^{-1})	β^{Tyr} (nm)	G_{Iso}^0 (eV)	ε_0	ε_0^W	ε_0^Y		χ^2
MCAD Method A	1164	7.04	0.738	1.78	0.677	1.63	6.23	4.22	2.54	2.27		3.11×10^{-3}
Method B	1135	4.20	0.786	4.78	0.606	1.18	6.18	3.29	2.71	2.13		1.25×10^{-2}
Flavodoxin[b] WT	3090	55.6	0.772	2460	9.64	0.676	7.67	5.85				
Flavodoxin[b] Y97F								4.78				
Flavodoxin[b] W59F								4.04				
Flavodoxin[b] Y97F/W59F								2.28				
AppA[c] WT	2304	18.1	0.539	2661	6.25	2.74	8.53	29.0				
AppA[c] W104F								13.7				
AppA[c] Y21F								2.45				
FMN-bp[d]	1016	21.0	0.570	197	6.64	0.00	8.97	9.86				
FMN-bp[e]	1016	21.0	0.663	197	6.25	0.499	9.22	8.03				

[a] Physical constants contained in KM theory were determined by the observed fluorescence dynamics. The meaning of the constants are explained in Eq. (1) and below Eq. (1).
[b] Data taken from Ref. [47].
[c] Data taken from Ref. [23].
[d] Data taken from Ref. [25].
[e] Data taken from Ref. [24].

Table 5
Mean physical quantities over MD time range and energy gap law.[a]

ET donor	R_j[b]	$\ln k_{ET}^j$[c]	λ_S^{qj}[d]	ES_j[e]	$-e^2/\varepsilon_0^q R_j$[f]	ΔG_q^{0}[g]	$-\Delta G_T^0(j)$[h]	$-\Delta G_T^0(j)/\lambda_S^{qj}$	$\ln k_{ET}^j/\lambda_S^{qj}$
Trp47	2.68	−17.90	1.25	−0.949	−0.163	0.744	0.368	0.296	−14.4
Trp156	1.00	1.12	0.66	−0.842	−0.545	0.744	0.643	0.977	1.7
Trp165	2.08	−23.77	1.22	−0.479	−0.210	0.744	−0.055	−0.045	−19.6
Trp307	3.20	−31.20	1.26	−0.359	−0.137	0.744	−0.248	−0.197	−24.7
Tyr32	2.29	−34.31	1.32	−0.625	−0.191	1.544	−0.727	−0.550	−25.9
Tyr38	1.64	−43.31	1.27	−0.370	−0.266	1.544	−0.908	−0.712	−34.0
Tyr79	2.58	−36.06	1.34	−0.573	−0.170	1.544	−0.802	−0.600	−27.0
Tyr104	3.41	−60.74	1.36	−0.019	−0.128	1.544	−1.396	−1.024	−44.5
Tyr110	2.54	−49.22	1.34	−0.262	−0.172	1.544	−1.109	−0.831	−36.9
Tyr123	1.29	−39.96	1.23	−0.426	−0.340	1.544	−0.778	−0.634	−32.6
Tyr148	2.97	−57.39	1.35	−0.086	−0.147	1.544	−1.310	−0.970	−42.5
Tyr166	1.69	−38.27	1.28	−0.601	−0.259	1.544	−0.684	−0.535	−29.9
Tyr267	3.42	−51.95	1.36	−0.307	−0.128	1.544	−1.109	−0.813	−38.1
Tyr302	2.29	−22.37	1.32	−1.168	−0.191	1.544	−0.185	−0.140	−16.9
Tyr317	2.74	−96.36	1.34	0.815	−0.160	1.544	−2.200	−1.637	−71.7
Tyr318	2.82	−84.22	1.35	0.603	−0.155	1.544	−1.992	−1.480	−62.6
Tyr325	2.55	−37.55	1.34	−0.625	−0.172	1.544	−0.748	−0.560	−28.1
Tyr350	3.19	−33.76	1.36	−0.797	−0.137	1.544	−0.610	−0.449	−24.9
Tyr362	1.42	−26.23	1.25	−0.856	−0.309	1.544	−0.380	−0.304	−21.0
Tyr365	0.99	0.18	0.14	−1.107	−0.695	1.544	0.258	1.834	1.3
Tyr384	3.50	−93.75	1.37	0.645	−0.125	1.544	−2.063	−1.511	−68.7

[a] The physical quantities are means of 20,000 snapshots for MD calculation time. Notations for the physical quantities are indicated in Eq. (1) in text.
[b] Center-to-center distance in unit of nm.
[c] k_{ET} is expressed in unit of ps^{-1}.
[d] Reorganization energy is given by Eq. (2).
[e] Net ES energies are given by Eq. (5) in unit of eV.
[f] ES energy between donor and acceptor is given by $-e^2/\varepsilon_0^q R_j$ in Eq. (1) (eV).
[g] $\Delta G_q{}^\circ$ is given by Eq. (3).
[h] The total free energy gap is given by Eq. (12) in unit of eV.

When λ_S^{qj} appreciably varies with the ET donors, the following modified energy gap law may be useful.

$$\frac{(\ln k_{ET}^j)}{\lambda_S^{qj}} \propto -\left\{\frac{1+\Delta G_T^0(j)}{\lambda_S^{qj}}\right\}^2 \quad (14)$$

Table 5 lists the values of physical quantities needed for the plots of the 21 ET donors. Fig. 14A demonstrated the original energy gap law given by Eq. (13), and in Fig. 14B shows the modified energy gap law, according to Eq. (14). In Fig. 14A $\ln k_{ET}^j$ increased with $-\Delta G_T^0(j)$. The red solid line denotes an approximate parabolic function of $\ln k_{ET}^j$ against $-\Delta G_T^0(j)$, $Y = -5.0414X^2 + 24.89X - 16.982$, where Y is $\ln k_{ET}^j$, and X, $-\Delta G_T^0(j)$. The value of $\Delta G_T^0(j)$ at the maximum ET rate was 2.5 eV. In Fig. 14B $\Delta G_T^0(j)/\lambda_S^{qj}$ was plotted against $\Delta G_T^0(j)/\lambda_S^{qj}$. The red solid line indicates an approximate parabolic function, $Y = -3.1043X^2 + 19.284X - 13.188$, where the Y is $\ln k_{ET}^j/\lambda_S^{qj}$, and X, $\Delta G_T^0(j)/\lambda_S^{qj}$. In the modified energy gap law $\ln k_{ET}^j/\lambda_S^{qj}$ displayed a maximum at 1.5 of $\Delta G_T^0(j)/\lambda_S^{qj}$, whilst no such maximum displayed in the normal energy gap law.

4. Discussion

MCAD is a flavoenzyme, which is different from electron transport proteins, such as FMN-bp, and flavodoxins. The Iso of FAD was buried in the protein and surrounded by rigid amino acids. Substrates of MCAD are very hydrophobic, being medium chain acyl-CoA, only one amino acid (Asp133) among 29 amino acids that exists near Iso (within 0.6 nm) is ionic. The low ε_0 in MCAD may be ascribed to these characteristics of the protein. The major H-bonds formed between Iso and Tyr123, Val125, Thr126 and Thr158. It is of interest that some of the geometrical factors, such as R_c and interplanar angle between Iso and the aromatic amino acids displayed a high correlation with the other geometrical factors. Such two aromatic amino acids with a high correlation coefficient are located at distant places in the MCAD protein and do not seem to have any relationship between them. Unless this simply represents a stochastic chance event, this suggests that motions are cooperative or synchronized with each other at some places in the MCAD.

Such cooperative motions may be related to ET rates. Table 6 lists the correlation coefficients between ET rates and geometrical factors as R_c or net ES energy for six fastest donors. ET rate of Trp156 was fastest and then follow by Tyr365, Trp47, Tyr302, Tyr165, and Tyr362, respectively. Quite good linear relations in Trp156 were obtained with the correlation coefficients ($r = -0.52$ for R_c and $r = -0.64$ for net ES energy). The correlation of ET rate with net ES energy was better than one with R_c of Trp156. The correlation coefficients between ET rate and net ES energies (ES_j) were always quite high in the all donors, whereas the coefficients between ET rate and R_c were negligible except for Tyr362. In Tyr362 ET rate may be correlated with R_c of other donors in addition to R_c of Tyr362 itself, though the ET rate was low. These results suggest that net ES energies are more important for ET rate in MCAD, which is in accord with the previous works [10,27].

The maximum rate was obtained with the approximate parabola function at $-\Delta G_T^0(j) = 2.5$ eV, which was much greater than those of flavodoxin (0.9 eV) [47] and FMN binding protein (0.16 eV) [27]. The extraordinary high value of $-\Delta G_T^0(j)$ at the maximum rate in Trp156 with fastest ET rate may be ascribed to very low dielectric constant of the entire protein, accordingly highest net ES energy in magnitude (−0.84 eV) in MCAD among three protein systems (−0.08 eV in FMN binding protein [27], −0.02 eV in flavodoxin [47]). The highest value of $-\Delta G_T^0(j)$ may be also ascribed to lowest value of G_{Iso}^0 (6.2 eV in MCAD, 6.8 eV in FMN binding protein [27], and 7.7 eV in flavodoxin [47]).

The redox potential of FAD in the ground state of MCAD has been calculated, by means of combined quantum mechanical and molecular mechanical simulation [37], to be −30 mV whilst the experimental value is −135 mV. In this work the O4, N3H and O2 are reported to form H-bonds with Thr158, Tyr133 and Val125, respectively, which is in accordance with the present work (see Fig. 10A). The vibrational frequency and effect of the H-bond on the C4=O4

Table 6
Correlation coefficient between ET rate and related quantity.[a]

Rate Trp156		Rate Tyr365		Rate Tyr47		Rate Tyr302		Rate Tyr165		Rate Tyr362	
R_c156	−0.518	Net365	−0.837	Net47	−0.949	Net302	−0.642	Net165	−0.630	R_c47	−0.525
Net156	−0.638	Net384	−0.731	Net156	−0.690	Net317	−0.744	Net123	−0.614	R_c165	−0.548
Net165	−0.761									R_c302	−0.527
										R_c318	−0.517
										R_c325	−0.562
										R_c350	−0.521
										R_c362	−0.650
										Angle362	0.511
										Angle384	0.544

[a] The correlation coefficients (Pearson) with greater than 0.5 are listed in the table. R_c, Angle, and Net denote center-to-center distance between Iso and a donor, inter-planar angle between Iso and a donor, net ES energy (ES_j). Numbers beside these quantities indicate the residue numbers, of which amino acids (Trp or Tyr) are shown in Table 5. Order of ET rates were Trp156, Tyr47, Tyr302, Tyr165, and Tyr362 (see Table 5).

vibrational frequency in MCAD have also been studied before by Resonance Raman and NMR spectroscopies [38].

Agreement between the observed and calculated decays was not very good. The value of χ^2 was 3.11×10^{-3} in MCAD using decay functions (Method A), which are compared to those in FMN binding proteins, 2.49×10^{-3} [27], and in flavodoxin 9.60×10^{-4} [47]. The significant deviation seems to be caused by the marked non-exponential nature of the observed decay in MCAD, in which ratio of the longest lifetime to the shortest one was as much as 140, whilst the ratios were 9.0 in WT FMN binding protein [27], 16 in Y97F flavodoxin, and 17 in W59F flavodoxins [47]. The present method

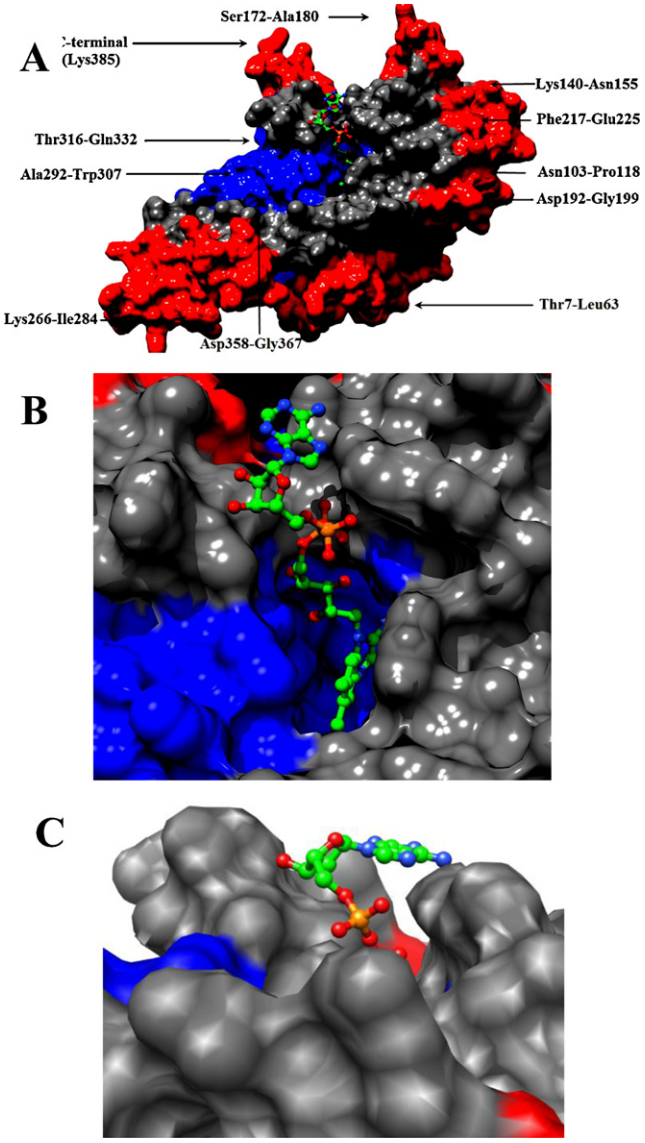

Fig. 9. Rigid and flexible parts of MCAD. The rigid (blue) and flexible (red) amino acids, based on the RMSF residual values (see Fig. 8) (A). The close view of the Iso binding site. Iso is buried inside the protein (B). The adenine binding site, which is exposed into water layer (C). (For interpretation of the references to color in this figure legend, the reader is referred to the web version of the article.)

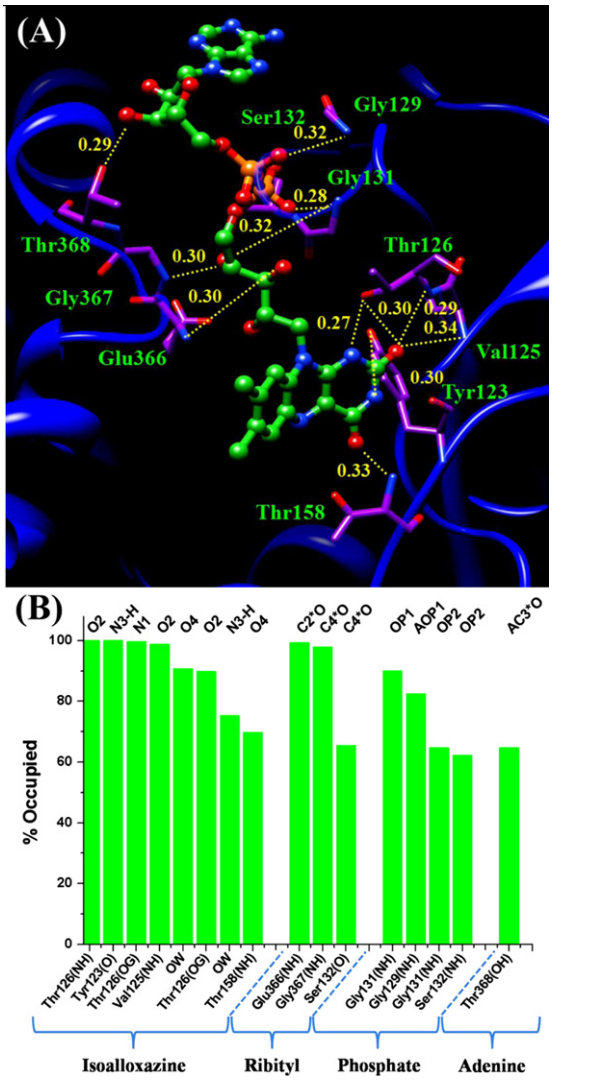

Fig. 10. H-bond formation between FAD and the surrounding MCAD amino acid residuess. (A) Schematic representation of the H-bonds between FAD and the neighboring amino acids with distances annotated in nanometers. (B) The percent occupation pattern of H-bonds (see Chart 1 for atom notations of FAD).

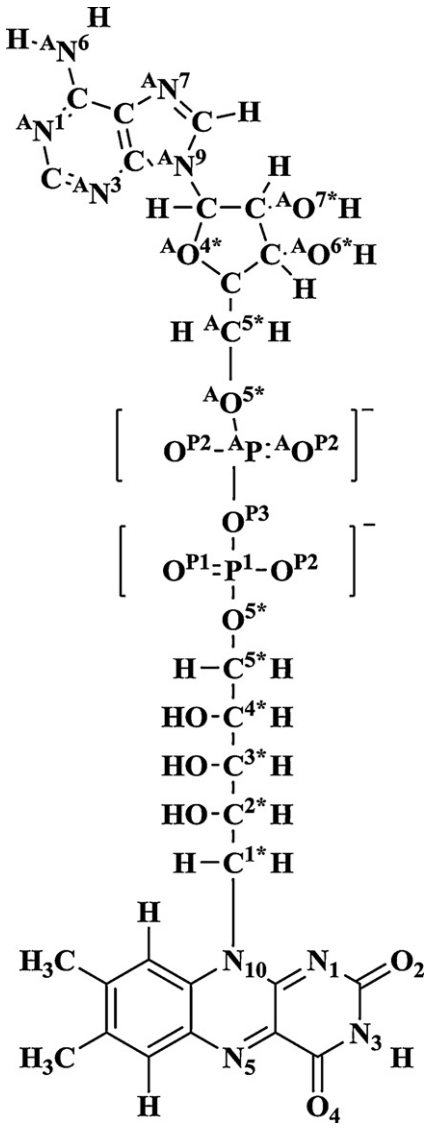

Chart 1. Chemical structure of FAD including the atomic numbering.

may not be good enough to simulate such high non-exponential decays. One of possible reason for it may be that any of static dielectric constants may be time-dependent, not constant. If a time-dependent dielectric constant is introduced, then fluctuation of ET rate with time may be enhanced, and accordingly the high non-exponential decay can be reproduced by the present method.

The energy gap law has been examined by many workers [10,35–38] in solution to test the Marcus theory [13–15], and especially for ET in the inverted region, which is critical for the Marcus theory. Rehm and Weller [39,40] systematically investigated the energy gap law in solution, but could not succeed to find it. Later Close et al. [41], and Mataga et al. [42,43] reported the ET phenomena in the inverted region. The energy gap law in proteins was first experimentally demonstrated in the reaction center of the purple bacterium, *Rhodobacter sphaeroides* by Gunner and Dutton [44], and the plant photosystem I and in the reaction center of the purple bacterium by Iwaki et al. [45]. In these systems, the ET takes place in the normal regions. The energy gap law in flavoproteins has been investigated in wild type flavodoxin and its mutated isoforms by Lugsanangarm *et al.* [46,47] and in wild type FMN-bp and four mutated FMN-bp systems by Nunthaboot et al. [27]. The ET in these flavoproteins also took place in the normal region.

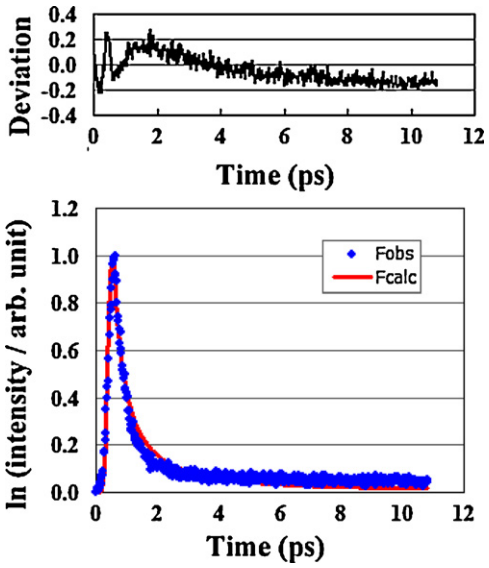

Fig. 11. Fluorescence decay of Iso in MCAD. The observed and calculated decays were obtained by Method B. F_{obs} and F_{calc} in the insert mean $F^c_{obs}(t)$ and $F^c_{calc}(t)$ given by Eqs. (9) and (10), respectively. The upper panel shows the deviation between the observed fluorescence ($F^c_{obs}(t)$) and the calculated ($F^c_{calc}(t)$). $F^c_{calc}(t)$ were calculated with the best-fit ET parameters determined by Method B (see Table 4). (For color in this figure, the reader is referred to the web version.)

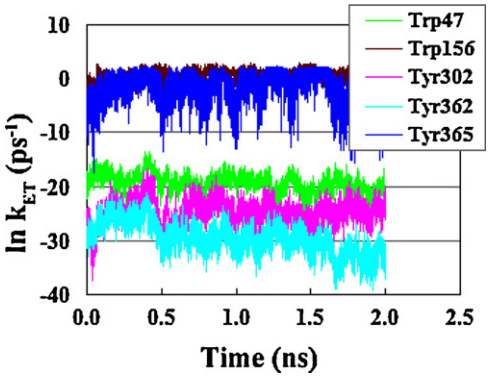

Fig. 12. Time-dependent changes in the ET rates from the five selected aromatic amino acids to Iso*. ET rates were calculated with ET parameters determined by Method B.

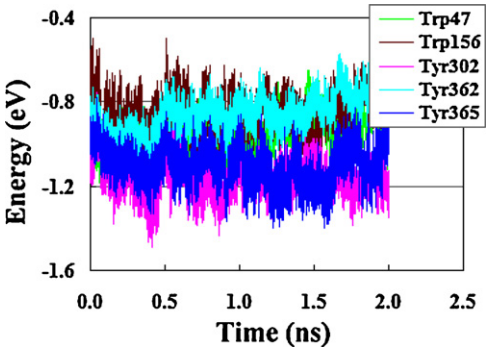

Fig. 13. Net ES energy between photoproducts and the other ionic groups in the MCAD Protein. The ES energies were obtained by Eq. (5) with $\varepsilon_0 = 3.29$ determined by Method B (see Table 4).

Acknowledgments

This work was supported by The Royal Golden Jubilee Ph.D. Program (3.C.CU/50/S.1), from Chulalongkorn University and The

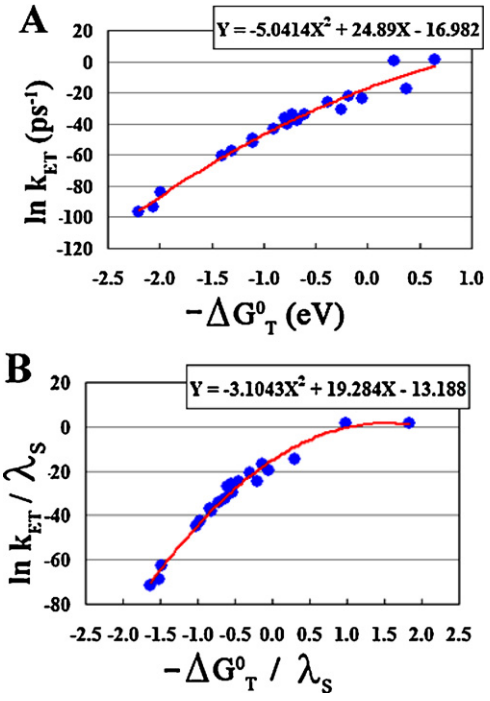

Fig. 14. Energy gap law of ET in MCAD Panel A shows the original energy gap law expressed by Eq. (13) and panel B the modified energy gap law expressed by Eq. (14). The values of $\Delta G_T^0(j)$ and λ_S^{qj} are expressed in eV unit. The insert in panel A shows an approximate parabolic function between Y ($\ln k_{ET}^j$) and X ($\Delta G_T^0(j)$), and the insert in panel B an approximate parabolic function between Y ($\ln k_{ET}^j/\lambda_S^{qj}$) and X ($\Delta G_T^0(j)/\lambda_S^{qj}$). These functions are indicated with solid red lines. (For interpretation of the references to color in this figure legend, the reader is referred to the web version of the article.)

Thailand Research Fund (TRF). We thank The Higher Education Research Promotion and National Research University Project of Thailand, Office of the Higher Education Commission (HR1155A). Thanks are given to Computational Chemistry Unit Cell, Chulalongkorn University and the National Electronics and Computer Technology Center (NECTEC). The Thai Government Stimulus Package 2 (TKK2555) under the Project for Establishment of Comprehensive Center for Innovative Food, Health Products and Agriculture is acknowledged.

Appendix A. Supplementary data

Supplementary data associated with this article can be found, in the online version, at doi:10.1016/j.jphotochem.2011.09.010.

References

[1] J.J. Kim, R. Miura, J. Biochem. 271 (2004) 483–493.
[2] S. Ghisla, C. Thorpe, J. Biochem. 271 (2004) 494–508.
[3] N. Gregersen, P. Bross, B.S. Andresen, J. Biochem. 271 (2004) 470–482.
[4] J.J. Kim, M. Wang, R. Paschke, Proc. Natl. Acad. Sci. U. S. A. 90 (1993) 7523–7527.
[5] Y. Nishina, K. Sato, K. Shiga, S. Fujii, K. Kuroda, R. Miura, J. Biochem. 111 (1992) 699–706.
[6] R. Miura, Y. Nishina, S. Fuji, K. Shiga, J. Biochem. 119 (1996) 512–519.
[7] N. Mataga, H. Chosrowjan, Y. Shibata, F. Tanaka, Y. Nishina, K. Shiga, J. Phys. Chem. B 104 (2000) 10667–10677.
[8] N. Mataga, H. Chosrowjan, S. Taniguchi, F. Tanaka, N. Kido, M. Kitamura, J. Phys. Chem. B 106 (2002) 8917–8920.
[9] H. Chosrowjan, S. Taniguchi, N. Mataga, F. Tanaka, D. Todoroki, M. Kitamura, J. Phys. Chem. B 111 (2007) 8695–8697.
[10] H. Chosrowjan, S. Taniguchi, N. Mataga, T. Nakanishi, Y. Haruyama, S. Sato, M. Kitamura, F. Tanaka, J. Phys. Chem. B 114 (2010) 6175–6182.
[11] A. Karen, M.T. Sawada, F. Tanaka, N. Mataga, Photochem. Photobiol. 45 (1987) 49–54.
[12] D.P. Zhong, A.H. Zewail, Proc. Natl. Acad. Sci. U. S. A. 98 (2001) 11867–11872.
[13] R.J. Marcus, J. Chem. Phys. 24 (1956) 969–978.
[14] R.A. Marcus, J. Chem. Phys. 24 (1956) 979–989.
[15] R.A. Marcus, N. Sutin, Biochim. Biophys. Acta 811 (1985) 265–322.
[16] C.C. Moser, J.M. Keske, K. Warncke, R.S. Farid, P.L. Dutton, Nature 355 (1992) 796–802.
[17] M. Bixon, J. Jortner, J. Phys. Chem. 95 (1991) 1941–1944.
[18] M. Bixon, J. Jortner, J. Phys. Chem. 97 (1993) 13061–13066.
[19] M. Bixon, J. Jortner, J. Cortes, H. Heitele, M.E. Michelbeyerle, J. Phys. Chem. 98 (1994) 7289–7299.
[20] T. Kakitani, N. Mataga, J. Phys. Chem. 89 (1985) 8–10.
[21] H.B. Gray, J.R. Winkler, Annu. Rev. Biochem. 65 (1996) 537–561.
[22] D.S. Bendall, Protein Electron Transfer, BIOS Scientific Publishers Ltd., Oxford, 1996.
[23] N. Nunthaboot, F. Tanaka, S. Kokpol, J. Photochem. Photobiol. A: Chem. 209 (2010) 79–87.
[24] N. Nunthaboot, F. Tanaka, S. Kokpol, H. Chosrowjan, S. Taniguchi, N. Mataga, J. Photochem. Photobiol. A: Chem. 201 (2009) 191–196.
[25] N. Nunthaboot, F. Tanaka, S. Kokpol, H. Chosrowjan, S. Taniguchi, N. Mataga, J. Phys. Chem. B 112 (2008) 13121–13127.
[26] N. Nunthaboot, F. Tanaka, S. Kokpol, J. Photochem. Photobiol. A: Chem. 207 (2009) 274–281.
[27] N. Nunthaboot, S. Pianwanit, S. Kokpol, F. Tanaka, Phys. Chem. Chem. Phys. 13 (2011) 6085–6097.
[28] V.V. Skakun, M.A. Hink, A.V. Digris, R. Engel, E.G. Novikov, V.V. Apanasovich, A.J.W.G. Visser, Biophys. J. 34 (2005) 323–334.
[29] D.A. Case, T.A. Darden, T.E. Cheatham III, C.L. Simmerling, J. Wang, R.E. Duke, R. Luo, M. Crowley, R.C. Walker, W. Zhang, K.M. Merz, B. Wang, S. Hayik, A. Roitberg, G. Seabra, I. Kolossváry, K.F. Wong, F. Paesani, J. Vanicek, X. Wu, S.R. Brozell, T. Steinbrecher, H. Gohlke, L. Yang, C. Tan, J. Mongan, V. Hornak, G. Cui, H.D. Mathews, M.G. Seetin, C. Sagui, V. Babin, P.A. Kollman, AMBER10, University of California, San Francisco, 2008.
[30] M.J. Frisch, G.W. Trucks, H.B. Schlegel, G.E. Scuseria, M.A. Robb, J.R. Cheeseman, J.J.A. Montgomery, T. Vreven, K.N. Kudin, J.C. Burant, J.M. Millam, S.S. Iyengar, T. J., V. Barone, B. Mennucci, M. Cossi, G. Scalmani, N. Rega, G.A. Petersson, H. Nakatsuji, M. Hada, M. Ehara, K. Toyota, R. Fukuda, J. Hasegawa, M. Ishida, T. Nakajima, Y. Honda, O. Kitao, H. Nakai, M. Klene, X. Li, J.E. Knox, H.P. Hratchian, J.B. Cross, C. Adamo, J. Jaramillo, R. Gomperts, R.E. Stratmann, O. Yazyev, A.J. Austin, R. Cammi, C. Pomelli, J.W. Ochterski, P.Y. Ayala, K. Morokuma, G.A. Voth, P. Salvador, J.J. Dannenberg, V.G. Zakrzewski, S. Dapprich, A.D. Daniels, M.C. Strain, O. Farkas, D.K. Malick, A.D. Rabuck, K. Raghavachari, J.B. Foresman, J.B. Ortiz, Q. Cui, A.G. Baboul, S. Clifford, J. Cioslowski, B.B. Stefanov, G. Liu, A. Liashenko, P. Piskorz, I. Komaromi, R.L. Martin, D.J. Fox, T. Keith, M.A. Al-Laham, C.Y. Peng, A. Nanayakkara, M. Challacombe, P.M.W. Gill, B. Johnson, W. Chen, M.W. Wong, C. Gonzalez, J.A. Pople, Gaussian03, Pittsburgh, PA, 2003.
[31] U. Essmann, L. Perera, M. Berkowitz, T. Darden, H. Lee, L. Pedersen, J. Chem. Phys. 103 (1995) 8577–8593.
[32] D.A. Case, T.E. Cheatham 3rd, T. Darden, H. Gohlke, R. Luo, K.M. Merz Jr., A. Onufriev, C. Simmerling, B. Wang, R.J. Woods, J. Comput. Chem. 26 (2005) 1668–1688.
[33] F. Tanaka, R. Rujkorakarn, H. Chosrowjan, S. Taniguchi, N. Mataga, Chem. Phys. 348 (2008) 237–241.
[34] F. Tanaka, H. Chosrowjan, S. Taniguchi, N. Mataga, K. Sato, Y. Nishina, K. Shiga, J. Phys. Chem. B 111 (2007) 5694–5699.
[35] V. Vorsa, T. Kono, K.F. Willey, N. Winograd, J. Phys. Chem. B 103 (1999) 7889–7895.
[36] E.R. Henry, R.M. Hochstrasser, Proc. Natl. Acad. Sci. U. S. A. 84 (1987) 6142–6146.
[37] S. Bhattacharyya, M.T. Stankovich, D.G. Truhlar, J. Gao, J. Phys. Chem. A 111 (2007) 5729–5742.
[38] Y. Nishina, K. Sato, R. Miura, K. Matsui, K. Shiga, J. Biochem. 124 (1998) 200–208.
[39] D. Rehm, A. Weller, B. Bunsen, Ber. Bunsenges, Phys. Chem. 73 (1969) 834–839.
[40] D. Rehm, A. Weller, Israel J. Chem. 8 (1970) 259–271.
[41] G.L. Closs, L.T. Calcaterra, N.J. Green, K.W. Penfield, J.R. Miller, J. Phys. Chem. 90 (1986) 3673–3683.
[42] N. Mataga, S. Taniguchi, H. Chosrowjan, A. Osuka, N. Yoshida, Photochem. Photobiol. Sci. 2 (2003) 493–500.
[43] N. Mataga, S. Taniguchi, H. Chosrowjan, A. Osuka, K. Kurotobi, Chem. Phys. Lett. 403 (2005) 163–168.
[44] M.R. Gunner, P.L. Dutton, J. Am. Chem. Soc. 111 (1989) 3400–3412.
[45] M. Iwaki, S. Kumazaki, K. Yoshihara, T. Erabi, S. Itoh, J. Phys. Chem. 100 (1996) 10802–10809.
[46] K. Lugsanangarm, S. Pianwanit, S. Kokpol, F. Tanaka, H. Chosrowjan, S. Taniguchi, N. Mataga, J. Photochem. Photobiol. A: Chem. 217 (2011) 333–340.
[47] K. Lugsanangarm, S. Pianwanit, S. Kokpol, F. Tanaka, H. Chosrowjan, S. Taniguchi, N. Mataga, J. Photochem. Photobiol. A: Chem. 219 (2011) 32–41.